The effect of redox conditions and bioirrigation on nitrogen

2 isotope fractionation in marine sediments

J. Rooze[#] and C. Meile^{*} Department of Marine Sciences, The University of Georgia, Athens GA 30602, USA #jurjen@uga.edu *cmeile@uga.edu

Abstract

23

24

25

26

27

28

29

30

31

32

33

34

35

36

37

38

39

Nitrogen isotopic signatures of sources and sinks of fixed nitrogen (N) can be used to constrain marine nitrogen budgets. However, the reported fractionation during benthic N₂ production varies substantially. To assess the range and mechanisms responsible for such observations, we conducted a model study to evaluate the extent to which nitrification, denitrification, and anaerobic ammonium oxidation contribute to the isotopic composition of in situ N₂ production. Different hydrodynamic regimes were taken into account, ranging from bioirrigation to diffusion-dominated transport. The benthic redox conditions were found to control the N isotope effect, which under reducing conditions is driven by fractionation during nitrification and anaerobic ammonium oxidation and under oxidizing conditions by fractionation during denitrification. Environmental parameters, such as the mineralization rate, the bioirrigation intensity, and chemical composition of the overlying water affect the benthic redox zonation and therefore also the benthic N isotope effect. The N isotope effect of benthic N₂ production was computed for a wide range of bioirrigation intensities and mineralization rates, and found to be approximately -3\% for commonly encountered conditions. This value is similar to previous estimates of the global N isotope effect of benthic N₂ production, and further constrains the relative importance of water column vs. benthic N₂ production.

40 41

42

43

44

45

46

47

48

Introduction

The availability of nitrogen (N) is considered one of the main controls of primary production in the ocean (Sarmiento and Gruber, 2006). Marine fixed N inventories are regulated mainly by microbial processes, which can induce N isotope effects by consuming or producing ¹⁴N and ¹⁵N species at slightly different rates. Therefore, the contributions from different sources and sinks to the bioavailable oceanic N pool can not only be determined from measured fluxes, but also constrained from their isotopic signatures (Montoya, 2008).

4950

Globally, nitrogen fixation is the largest source and N₂ production through denitrification (DNF) and anaerobic ammonium oxidation (anammox) represent the major sinks of

bioavailable N in the ocean. N fixation introduces N with a δ^{15} N of $-1 \pm 1\%$ (δ^{15} N = 53 $\{[^{15}N/^{14}N] / [^{15}N/^{14}N]_{standard} - 1\} * 1000\%$; Minagawa and Wada, 1986; Carpenter et al., 54 1997). Anammox is carried out by chemolithoautotrophic bacteria that gain energy from 55 the reaction of ammonium (NH_4^+) with NO_2^- to N_2 , with an N isotope effect of -16% for 56 NO₂⁻ reduction and approximately -26% for NH₄⁺ oxidation (Brunner et al. 2013). 57 During DNF, nitrate (NO₃⁻) is reduced through several intermediates, including nitrite 58 59 (NO₂⁻) to dinitrogen gas (N₂). Although fractionation can occur during each step, the overall N isotope effect of the DNF pathway is affected most by the step in which a 60 61 nitrogen-oxygen bond of a nitrate ion bound to nitrate reductase is cleaved (Shearer et al., 1991). In laboratory studies with marine denitrifying bacteria, fractionation by -5 to 62 63 -30% has been measured, depending on the specific denitrifier species and experimental 64 conditions (Wellman et al., 1968; Granger et al., 2008; Kritee et al., 2012).

65

66

67

68

69

70

71

72

73

74

75

76

77

78

79

80

81

82

Strong N isotope fractionation of $-25 \pm 5\%$ has been reported to occur during N_2 production in oxygen minimum zones (Brandes et al., 1998; Altabet et al., 1999; Sigman et al., 2003). Due to this fractionation, NO_x (NO₂⁻ + NO₃⁻) tends to become locally enriched in 15N, which counters the discrimination against the preferential consumption of ¹⁴N and diminishes the effect on the bulk oceanic fixed δ^{15} N (Deutsch *et al.*, 2004). Thus, the apparent enrichment factor of water-column N₂ production is likely substantial, but less negative than the organism-level N isotope effect. In sediments the apparent N isotope effect was thought to be close to zero, since initial studies showed that the bottom water δ¹⁵N-NO_x did not change during incubation experiments (Brandes and Devol, 1997; Brandes and Devol, 2002; Lehmann et al., 2004). More recent studies have called the assumption of negligible N isotope fractionation into question. Firstly, fractionation during nitrification can produce light NO_x substrate for N₂ production and lead to exchange fluxes of heavy reduced N (NH₄⁺ + dissolved organic nitrogen [DON]) from the sediment to the overlying water, which then increases the ocean fixed $\delta^{15}N$ (Granger et al., 2011; Alkhatib et al., 2012). Secondly, NO_x exchange fluxes have been found to directly communicate the benthic N isotope effect to the overlying water (e.g. Dale et al. 2014), which is consistent with observations in incubation experiment showing that N

isotope fractionation during DNF led to heavier bottom water NO₃⁻ (Dähnke and Thamdrup, 2013).

85

8687

88

89

90

91

92

93

94

95

96

97

98

99

100

101

102

103

104

83

84

In this study, we assess N isotope fractionation in sediments that are inhabited in bottom dwelling organisms. In particular near-shore environments are commonly inhabited by benthic infauna, which often are critical in shaping their habitat (Meysman et al., 2006a; Archer and Devol, 1992; Volkenborn et al., 2007). They enhance solute transport in sediments (Meile and Van Cappellen, 2003), increase benthic mineralization rates (Aller and Aller, 1998; Kristensen, 2001; D'Andrea and DeWitt, 2009), and promote higher coupled nitrification-N₂ production rates (Grundmanis and Murray, 1977; Na et al., 2008). The study of sediment N cycling is particularly relevant on continental shelves, which host 50 - 65% of the global benthic N₂ production (Middelburg et al., 1997; Bianchi et al., 2012; Bohlen et al., 2012). Approximately 70% of continental shelf sediments are permeable (Emery, 1968), so that advective transport typically dominates solute transport (Hüttel et al., 2003). Flow circulating through such sediment may introduce NO₃⁻ that is only partially consumed in situ, leaving the efflux enriched in heavy N to potentially communicate the N isotope effect of N₂ production to the overlying water. Kessler et al. (2014) found that N₂ production in a column experiment with current-induced flow led to an N isotope effect of approximately -2.8\%. However, the effect of bioirrigation on benthic N isotope cycling has not yet been studied in detail. Here we present a mechanistic, early diagenetic process model to quantify the N isotope effect in sediment surrounding a burrow and identify the role of the redox conditions and advection induced by infauna in controlling the N isotope effect of benthic N₂ production.

105106

107

108

109

110

111

112

Methods

Reaction transport model

The mechanistic model simulated the effects of sediment early diagenesis in the presence of pumping infauna on the isotopic signature of benthic N fluxes. A 2D axisymmetric domain represented the physical 3D cylindrical environment surrounding a burrow, following the lugworm model of Meysman *et al.* (2006b). The domain radius was 10 cm,

which corresponds to a population density of ~32 individual organisms m⁻². The uppermost 2 cm of the domain represented the bottom water, overlying 20 cm of sediment. A burrow feeding pocket was implemented as a fluid injection site of radius 2.5 mm located at 15 cm depth, with a feeding funnel above it that had a 10 times higher permeability than the rest of the sediment (Jones and Jago, 1993; Riisgård and Banta, 1998).

The method described in Dornhoffer *et al.* (2015) was used to simulate fluid flow. In short, flow velocities were calculated using the Navier-Stokes and Darcy-Brinkman equations (Le Bars and Worster, 2006), accounting for pressure forces and shear stress in the momentum balance. Fluid was injected into the sediment at a constant rate by imposing a normal velocity on the boundary of the feeding pocket. Symmetry conditions with zero normal flow were imposed at the outer cylinder boundaries. Zero normal flow was imposed at the bottom of the domain, while the top boundary allowed for fluid to escape.

The steady-state distribution of dissolved species was described by the following mass balance equation:

$$0 = \nabla \cdot (\phi D_i \nabla C_i - \phi v C_i) + R \tag{1}$$

where D_i is the diffusion coefficient, C_i is the concentration, ϕ is the porosity (set to 1 in the overlying water), \mathbf{v} is the velocity vector, and R is the net reaction rate. The molecular diffusion coefficients D_i^{mol} were calculated following Boudreau (1997) at a temperature of 5°C and a salinity of 35. In the bottom water the diffusion coefficient was the sum of D_i^{mol} and the eddy diffusion coefficient calculated with the Reichardt equation (Boudreau, 2001a):

$$D_i = D_i^{mol} + \kappa z u^* \left[1 - \frac{11v}{zu^*} \tanh\left(\frac{zu^*}{11v}\right) \right]$$
 (2)

where κ is the dimensionless von Karman constant (0.4), z is the distance from the sediment-water interface, u^* is the shear velocity (set to 10^{-3} m s⁻¹), and v is the kinematic viscosity (10^{-6} m² s⁻¹). The diffusion coefficient in the sediment was corrected for tortuosity in the porous medium following Boudreau (1996):

$$D_i = \frac{D_i^{mol}}{(1 - 2\ln\phi)} \tag{3}$$

The reaction network (Table 1) described mineralization of dissolved organic matter (DOM) in the sediment with aerobic respiration, DNF, and dissimilatory iron oxide (Fe(OH)₃) and sulfate (SO₄²⁻) reduction. The various mineralization reactions of labile DOM with different electron acceptors use a first-order rate law with respect to DOM concentration (Table 1). NO₂⁻ was accounted for explicitly to implement anammox and to act as an intermediate in the DNF and nitrification reactions. Sulfide (HS⁻) and dissolved iron (Fe²⁺) can be reoxidized or form a FeS precipitate (Table 1). Reaction rates were set to zero in the overlying water, and processes such as dissimilatory nitrate reduction to ammonium, ammonium assimilation, or benthic primary production, which may become important in shallower waters, are not included. Strong mixing of the sediment by macrofauna was assumed to lead to a homogeneous distribution of solids in the sediment, and POM and Fe(OH)₃ concentrations were held constant over the domain depth.

The parameterization of the baseline simulation was based on literature values, and within the reported ranges adapted to the setting of Brandes and Devol (1997). The measured benthic exchange fluxes of inorganic N and the N_2 production rate were fitted by adjusting the benthic DOM production rate, the rate constants and half-saturation constants of nitrification, DNF, and anammox, and by adjusting the fractionation factors associated with NH_4^+ consumption during anammox and nitrification (Table 2). At the top of the domain, known concentrations were imposed. For this, the bottom water concentrations of O_2 and NO_3^- and the $\delta^{15}N$ of NO_3^- and organic matter reported by Brandes and Devol (1997) were used (Table 2). The concentrations in the oxygenated bottom water of reduced species NO_2^- , NH_4^+ , Fe^{2^+} , and HS^- were set to zero, and the DOM concentration was set to $50~\mu M$ (Lønborg and Søndergaard, 2009). The same concentrations were also imposed at the feeding pocket, except that respiration by the macrofauna was assumed to produce NH_4^+ and lead to a 60% oxygen drawdown in the fluid injected (Table 2). No flux conditions were imposed at the domain sides and bottom.

The model was implemented in COMSOL4.4 using the "Free and Porous Media Flow" and "Solute Transport" application modes. The domain was discretized with approximately 23,000 triangular elements, with element sizes ranging from about 60 μ m to 1 cm. The mesh was finest near the feeding funnel and sediment-water interface in order to resolve sharp concentration gradients accurately. All simulations were run dynamically to steady state.

Nitrogen isotope fractionation

For the dissolved N species separate state variables were included to account for 14 N and 15 N. N isotope fractionation occurred through multiplying rate constants of the 15 N species by fractionation factors, which are defined as $\alpha = (R^h/R^l) / (^{15}N/^{14}N)_{\text{substrate}}$, where R^h and R^l are the rates of reactions that consume 15 N and 14 N species, respectively (Table 1; Mariotti *et al.*, 1981). The fractionation factors were generally less than 1, reflecting enzymatic discrimination against heavy N (Table 2). The only exception was NO_2^- oxidation, which has an inverse N isotope effect (Casciotti, 2009).

The effect of the benthos on the isotopic composition of fixed N in the ocean is determined by the fluxes and isotopic composition of inorganic and organic N across the sediment-water interface. At steady-state the sum of these fluxes have to balance the magnitude and isotopic composition of the in situ N_2 production, since DNF and anammox are the only sinks of N in the model. Therefore, the isotopic composition of the in situ produced gas can be used to quantify the N isotope effect (ε_{sed}):

$$\varepsilon_{sed} = \left[\frac{\binom{15}{N}^{14}N}_{N_2 \ production} - 1 \right] * 10^3$$
(4)

where the N_2 production rates are defined as:

$$\frac{4}{3}R_2^i + R_6^{NO2i} + R_6^{NH4i} + 2R_6^{ii} \tag{5}$$

with *i*=h for ¹⁵N and 1 for ¹⁴N; *ii* denotes anammox using nitrite and ammonium that are both heavy or light, respectively (Table 1). Burial of organic N is not taken into account, since the flux is small compared to the benthic and water-column N₂ production rates (Brandes and Devol, 2002). 198

199 The model can be used to quantify the contribution of individual processes to the isotopic

200 composition of N₂ produced in the sediment and hence the overall benthic N isotope

201 effect,

$$\varepsilon_{sed} \approx \delta^{15} \text{N-N}_2 - \delta^{15} \text{N-NO}_{3,\text{bw}}$$
 (6)

where $\delta^{15}N$ - N_2 and $\delta^{15}N$ - $NO_{3,bw}$ are the isotopic composition of the in situ produced N_2

203 gas and NO₃⁻ in the overlying water, respectively. The isotopic composition of N₂

produced from different sources in the absence of fractionation can be approximated by:

$$\delta^{15} \text{N-N}_2 = f_1 \delta_1 + \dots + f_n \delta_n \tag{7}$$

where f_i refers to the fraction of source i (with a signature δ_i). Fractionation in the

206 conversion of substrate s to product p can be expressed as

$$\delta p \approx \delta s + \varepsilon.$$
 (8)

207 Combining equations 7 and 8 yields:

$$\delta_{N_2} = f_1 \delta_1 + f_1 \varepsilon_1 + \dots + f_n \delta_n + f_n \varepsilon_n = A + \sum f_i \varepsilon_i \tag{9}$$

Substitution into Eq. 6 shows that a simulation with all the fractionation factors (α , Table

209 2) set to 1, which turns off fractionation in the model, yields an apparent N isotope effect

210 (ε_{θ}) that accounts for sources with a different N isotopic composition (organic N and

bottom water NO_3 and is reflected in the parameter A (Eq. 9)

$$\varepsilon_0 \approx A - \delta^{15} \text{N-NO}_{3,\text{bw}}.$$
 (10)

Next simulations were run with a single fractionation factor having its original value and

all the others set to 1, which yields an apparent N isotope effect (ε_i) . The apparent N

214 isotope effect of individual processes ($\varepsilon_k = \varepsilon_j - \varepsilon_0$) can then be combined to yield the

215 overall benthic N isotope effect

$$\varepsilon_{sed} = \varepsilon_0 + \sum \varepsilon_k. \tag{11}$$

216

220

213

The effect of the areal bioirrigation intensity on benthic N isotope cycling was examined

by changing the pumping rate (Q, Table 2) and organism density, i.e. the domain radius.

219 Simulations with a burrowing depth of 5 cm were performed to analyze the impact of

shallow bioirrigation. The in situ DOM production rate ($F_{DOM,prod}$, Table 2), DOM

reactivity (k_{DOM} , Table 2), and the composition of the overlying water ($O_{2,bw}$ and $NO_{3,bw}$,

Table 2) were varied to evaluate the benthic N isotope effect in different environmental settings.

Finally, sediment N fractionation was quantified for a wide range of mineralization rates and areal bioirrigation intensities. The latter is the pumping rate of an individual organism (Q, Table 2) divided by the domain surface area ($A = \pi r^2$, Table 2). In total 198 simulations were carried out in which the bioirrigation intensity and mineralization rates were varied from 4.6 to 91.7 L m⁻² d⁻¹ and 0.36 to 29.73 mmol m⁻² d⁻¹, respectively. Since burrowing macrofauna are dependent on the availability of POM as food source (Künitzer *et al.*, 1992), sediment mineralization rates and bioirrigation intensities are often related. Two empirical relationships from literature were employed to provide a first order estimate of commonly encountered conditions, using the total sediment community oxygen consumption (SCOC) as a measure for the mineralization rate. The first relationship is based on an estimate of non-diffusive sediment O_2 uptake (see Eq. 1 in Meile and Van Cappellen, 2003), which we tentatively assume to be due to bioirrigation. Recasting that equation and assuming a negligible amount of O_2 in the sediment porewater yields:

$$\frac{Q}{A} = \frac{SCOC}{O_{2,bw}} \left(1 - \frac{1}{1.292 + 0.073 * SCOC} \right) * 1000$$
 (12)

- where Q/A is in L m⁻² d⁻¹, SCOC corresponds to the mineralization rate in mmol C m⁻²
- d^{-1} , and $O_{2,bw}$ is the oxygen bottom water concentration in μM (Table 2).
- 241 The second method uses the equation derived by Fennel et al. (2009), which estimates the
- benthic N_2 production rate (F_{N2} , mmol N m⁻² d⁻¹) as a function of SCOC:

$$F_{N2} = 0.086111 * SCOC + 0.17624 (13)$$

243 Results for simulations with particulate-to-dissolved organic matter conversion

 $(F_{DOM,prod}, Table 2)$ and pumping (Q) rates, which match the relationship between SCOC

and F_{N2} given in Eq. 13 were then identified. Since the sediment N_2 production in the

model is to a large extent dependent on the NO₃⁻ introduced through bioirrigation (see

results), this allows identification of the corresponding bioirrigation intensity.

Results

The distribution of solutes and reaction rates in the baseline simulation are shown in Fig. 1. O₂ was restricted to a plume surrounding the feeding pocket (Fig. 1a), limiting the volume where aerobic remineralization and nitrification (Fig. 1d) can take place. The zone of N₂ production through DNF and anammox (Fig. 1e), which are inhibited by O₂ and limited by NO_x availability (Fig. 1b), encapsulated this oxygenated zone. At a burrowing depth of 15 cm nearly all NO_x produced in situ or pumped into the sediment was ultimately reduced to N₂, while at a shallower burrowing depth of 5 cm the burrow-associated NO_x plume extended across the sediment-water interface (see contour lines in Fig. 1b), enabling a significant fraction of the injected NO_x to escape reduction to N₂. Modeled NH₄⁺ concentrations were suppressed at the depth of the feeding pocket due to high consumption by nitrification and anammox (Figs. 1c and f). The NO₃⁻ profile peaked at the feeding pocket depth, while the NO₂⁻ concentrations remained below 4 μM throughout the sediment domain. The lateral heterogeneity in the sediment allows the highest rates of aerobic and anaerobic processes to occur at the same depth (*e.g.* anammox and nitrite oxidation, Fig. 1f).

The benthic exchange fluxes measured by Brandes and Devol (1997) were reproduced in the baseline simulation. The modeled benthic O_2 uptake of 4.4 mmol m⁻² d⁻¹ and the magnitude and isotopic composition of the NH₄⁺ flux to the overlying water (Fig. 2a) matched their data. Bottom water NO₃⁻ with a measured δ^{15} N of 7.3‰ was pumped into the sediment and was reduced to NO₂⁻. A small fraction of relatively light NO₂⁻ was able to escape further reduction and fluxed out to the overlying water (Fig. 2a). The resultant net NO_x flux into the sediment of 7.5‰, combining an influx of bottom water nitrate of 7.3‰ with a nitrite efflux of 3.3‰, was slightly heavier than the bottom water NO₃⁻ and matched with the values reported in Brandes and Devol (1997). Denitrification of NO₂⁻ and anammox accounted for 63% and 37% of the benthic N₂ production, respectively. The N₂ production also matched that of Brandes and Devol (1997), but had a δ^{15} N of 5.2‰ compared to the reported 1 ± 4‰. Applying Eq. 4 the ε_{sed} value was -2.4‰.

Sensitivity analyses were performed by changing the pumping rate (Fig. 3a), burrow density and burrow depth (Fig. 3b), the reactivity of DOM (Fig. 3c), the bottom water O₂ and NO₃⁻ concentrations (Fig. 3d and e), and the POM to DOM conversion rate (Fig. 3f). Each panel shows the N_2 production rates (top) and the ε_{sed} values (bottom), which together determine the effect of benthic N₂ production on the isotopic composition of dissolved inorganic N in the overlying water. A lower pumping rate decreased the N₂ production rate and led to a higher expression of the N isotope effect of anammox and nitrification (Fig. 3a). Conversely, higher pumping rates enhanced the N₂ production and led to more fractionation due to DNF (Fig. 3a). Changing the domain radius, reflecting a different organism density, showed a similar pattern. Fractionation due to nitrification and anammox was more strongly expressed when the bioirrigation intensity was decreased (larger domain radius, Fig. 3b), while the fractionation induced by DNF was stronger when the bioirrigation intensity was increased (smaller domain radius). A shallower burrow depth of 5 cm reduced the N₂ production rate and increased the N isotope fractionation of nitrification, anammox, and DNF (compare left and right group in Fig. 3b).

Lowering the reactivity of DOM by two orders of magnitude (to $k_{DOM} = 2 * 10^{-7} \text{ s}^{-1}$, Fig. 3c) led to a strong degree of N isotope fractionation. Fractionation during NH₄⁺ oxidation made ε_{sed} less negative and thus had an apparent inverse N isotope effect. However, the effect on the isotopic composition of NO_x in the overlying water was small (Fig. 2b), since the N₂ production was very low (Fig. 3c, top panel). Lowering the reactivity of DOM by only one order of magnitude (to $k_{DOM} = 2 * 10^{-6} \text{ s}^{-1}$, Fig. 3c), led to a slightly lower N₂ production rate than in the baseline simulation. Fractionation during DNF had a large impact on ε_{sed} and led to heavier NO_x in the overlying water. A higher DOM reactivity ($k_{DOM} = 2 * 10^{-5} \text{ s}^{-1}$ and $k_{DOM} = 2 * 10^{-4} \text{ s}^{-1}$, Fig. 3c) had little effect on the N₂ production rate, but led to less N isotope fractionation during DNF and slightly more fractionation during NH₄⁺ oxidation and anammox. The isotopic composition of the benthic NO_x flux was similar to that of NO₃⁻ in the overlying water and had therefore a negligible effect on the δ^{15} N of NO_x in the overlying water (Fig. 2b). Changing the rate of DOM to POM conversion had a moderate effect on the benthic N₂ production rate

(Fig. 3f) and the contribution of individual processes on ε_{sed} values showed similar trends as changing the DOM reactivity.

The bottom water O_2 concentration had a moderate effect on the N_2 production rate, with maximum areal rates at 250 μ M (Fig. 3d). At higher O_2 concentrations, fractionation during DNF led to substantially more negative ε_{sed} values. The highest contribution of NH_4^+ oxidation and anammox to the isotope effect of benthic N_2 production was at relatively low O_2 concentrations of $50-100~\mu$ M. The bottom water NO_3^- concentrations had a substantial effect on the benthic N_2 production rates (Fig. 3e). The N isotope effect of NH_4^+ oxidation and anammox was stronger at low NO_3^- concentrations, while fractionation during DNF was stronger at high NO_3^- concentrations.

Changing the mineralization rate and bioirrigation intensity simultaneously gives insight in the expression of the benthic N isotope effect in different environments. The ε_{sed} values were most negative when either the irrigation intensity was high and the mineralization rate low or, conversely, the irrigation intensity low and the mineralization rate high (Fig. 4). Between these extremes, there was a relatively large region with ε_{sed} values between -2.1 and -4%. The two lines in Fig. 4 that tentatively indicate which mineralization rates may be most typical for different bioirrigation intensities (see methods section) were similar for low bioirrigation intensities, but differed more substantially at higher values. Nonetheless, both ε_{sed} values corresponding to these estimates of commonly encountered combinations of irrigation intensities and mineralization rates were generally less negative than -3.5%. A similar analysis conducted with a burrow depth of 5 cm (not shown) exhibited a similar pattern, but exhibited about 2-3% more negative ε_{sed} values.

Discussion

Benthic nitrogen processing and isotope fractionation

Macrofauna can pump bottom water to depths in the sediment that without bioirrigation would be anoxic. The simulated redox zonation with an oxic plume surrounding the feeding pocket and anoxic conditions in the remainder of the sediment (Fig. 1a) are in

line with studies on large burrowing macrofauna (Na et al., 2008; Volkenborn et al., 2010). The modeled solute profiles showed pronounced accumulation of NO₃⁻ and depletion of NH₄⁺ at the feeding pocket depth (Fig. 1c), which is qualitatively consistent with profiles measured at sites with large burrowing macrofauna (Grundmanis and Murray, 1977; Hüttel, 1990; Volkenborn et al., 2007). At the Puget Sound site studied by Brandes and Devol (1995, 1997), measured O₂ and NO₃⁻ concentrations approached zero in the uppermost centimeter of sediment, similar to the computed horizontally averaged concentration profiles (Fig. 1c), but no measurements were reported at greater depth in the sediment, where infauna present (Lie, 1968; Brandes and Devol, 1997; Nichols, 2003) may have affected O₂ and NO₃ concentrations. Sediment permeability and porosity constrains the environment in which bioirrigation can be a dominant transport process (Hüttel et al., 2003). However, since model simulations use an imposed pumping rate, the computed flow field is only impacted by spatial variations in permeability. The ten-fold higher permeability in the feeding funnel than in the bulk sediment leads to a slightly higher expulsion of porewater through this conduit. However, the overall effect on the benthic N exchange fluxes and expression of the N isotope effect was small $(\Delta \varepsilon = -0.1\%)$. Similarly, variations in porosity have only a minor impact on fluxes and fractionation (not shown).

For a given organism density (reflected in the domain size), the pumping rate controlled the benthic exchange fluxes of NO_x and O_2 , since the injected NO_x and O_2 were in most settings quantitatively consumed. For instance, in the baseline simulation all O_2 and nearly all NO_x from the plume were consumed before they could reach the sediment-water interface (Fig. 1b). Areal pumping rates, which are a combination of the density of burrowing organisms and the individual pumping rates, were the same in the simulations with a domain radius r = 10 cm and Q = 0.16, 0.62, and 1.86 mL min⁻¹ (Fig. 3a) and those with Q = 0.62 mL min⁻¹ and r = 20, 10, and 5.8 cm (Fig. 3b, burrow depth = 15 cm), respectively. The corresponding bar plots are nearly identical. This indicates that the areal bioirrigation intensity controls the magnitude and isotopic composition of the N fluxes.

The model simulations reproduced the benthic exchange fluxes reported by Brandes and Devol (1997) except that the isotopic composition of the in situ produced N₂ gas differed by 4‰ from the average measured value reported by Brandes and Devol (1997). Multiple factors could have played a role in causing this discrepancy. Firstly, determining N₂ fluxes is challenging due to the high background concentrations of N₂ in seawater (Hamersley and Howes, 2004), and uncertainties in isotopic signatures of fluxes can be substantial (± 4‰ in Brandes and Devol, 1997). Secondly, sediment N sources and sinks may be out of balance, while steady-state conditions were assumed in the model, which can lead to differences in modeled and observed benthic N fluxes and isotope effects. Finally, the model did not account for dissimilatory nitrate reduction to ammonium, connecting the oxidized and reduced dissolved inorganic N species, or for NH4+ assimilation, which could affect the isotopic composition of benthic DON exchange fluxes. Underestimating the efflux of heavy DON would result in an isotopically too heavy N₂ efflux in the model. Alkhatib et al. (2012) have argued that DON fluxes can play an important role in communicating benthic N isotope effects to the overlying water. However, this contribution remains poorly constrained as neither Alkhatib et al. (2012) nor Brandes and Devol (1997) reported the $\delta^{15}N$ and flux of DON separately from NH₄⁺.

In the sensitivity analysis the expression of the N isotope effect of individual processes (ε_i , Fig. 3) is largely controlled by the benthic redox conditions. More oxidizing conditions correspond to higher injection rates of oxic bottom water into the sediment (Q, Fig. 3a), higher organism densities (i.e. smaller domain radii, Fig. 3b), DOM with less reducing power (smaller k_{DOM} , Fig. 3c), more O_2 and NO_3^- in the bottom water (Figs. 3d and e), the production of less reducing DOM (Fig. 3f), while the opposite trends correspond to more reducing conditions. Under oxidizing conditions discrimination against heavy NO_3^- during DNF is more strongly expressed, whereas under reducing conditions discrimination against heavy NH_4^+ during NH_4^+ oxidation and anammox is more pronounced. This reflects that the expression of N isotope fractionation at the cell level is dependent on the fraction of the benthic reactant pool that is being consumed (Mariotti *et al.*, 1981; Lehmann *et al.*, 2004). Under oxidizing conditions the sediment resembles a closed system for NH_4^+ , consuming a larger fraction of the benthic NH_4^+

pool, and preventing the efflux of heavy NH_4^+ caused by fractionation during NH_4^+ oxidation and anammox to the overlying water. Meanwhile, the sediment resembles a more open system towards NO_3^- and simulations that showed stronger expression of the fractionation during NO_3^- reduction ($\varepsilon_{NO3,DNF}$) had NO_x plumes that extended from the feeding pocket to the sediment-water interface (e.g. Figs. 1b and 3b). The preferential consumption of light NO_x in the sediment will then lead to a flux of NO_x enriched in ^{15}N to the overlying water. Conversely, under more reducing conditions, the system becomes more open towards NH_4^+ as less O_2 is available to oxidize it, while it becomes more closed towards NO_3^- , minimizing the expression of the N isotope effect of DNF.

The expression of a benthic N isotope effect depends on the fractionation occurring at the cell level, as well as the coupling between different reactions that compete for substrates. The latter can lead to an apparent inverse N isotope effect on the overall benthic N_2 production, despite a fractionation factor $\alpha < 1$, as seen for NH_4^+ oxidation at low mineralization rates (Figs. 3c and f). Since fractionation during this reaction leads to heavier NH_4^+ and lighter NO_2^- , the inverse apparent N isotope effect (production of isotopically heavy N_2) can only occur when a large amount of NH_4^+ is converted to N_2 and a part of the produced NO_x escapes to the overlying water. This depends on the prevalent redox conditions, and requires anammox to be the dominant N_2 production pathway, propagating the heavy residual NH_4^+ signature into N_2 . When DNF dominates N_2 production (as is the case at higher mineralization rates in Figs. 3c and f), the δ_{N2} reflects largely the isotopic signature of the NO_2^- and a "normal" negative apparent N isotope effect of NH_4^+ oxidation is observed.

The impact of the benthic N isotope effect on the isotopic composition of fixed N in the overlying water is dependent on both ε_{sed} and the N₂ production rate. Thus, there is a stronger impact at high irrigation rates compared to conditions with low Q, as N₂ production increases with the higher input of NO₃⁻ (Fig. 3a). Similarly, there is a very strong N isotope effect at the lowest DOM reactivity, but the impact on fixed N in the overlying water is negligible due to the extremely low N₂ production rate (Fig. 3c). In Fig. 3e the N isotope effect of NH₄⁺ oxidation and anammox is stronger at lower NO₃⁻

bottom water concentrations. This is because at the same pumping rate less NO_3^- is injected, so that the N_2 production and its isotopic signature are more dependent on fractionation during NH_4^+ oxidation. At higher NO_3^- concentrations in the bottom water, the supply of NO_3^- to the sediment via bioirrigation increases. This stimulates N_2 production and lowers the relative contribution of NH_4^+ oxidation to the benthic nitrogen isotope effect (Fig. 3e).

The effect of solute transport on benthic nitrogen isotope fractionation

In bioirrigated sediment, N isotope cycling is dependent on the bioirrigation intensity and the burrowing depth (Figs. 3a and b). For shallow burrows, some of the injected NO_x is flushed out the sediment before it can be reduced, which significantly enhances the expression of the N isotope effect of DNF. A shallow burrow depth also increases the expression of the N isotope effect of nitrification and anammox (Fig. 3b). Rates of these processes are highest within and around the oxic plume (Figs. 1d and e). When the plume extends across the sediment-water interface a larger fraction of NH₄⁺ produced in the sediment by organic matter mineralization escapes to the overlying water (Fig. 3b) and allows for expression of the N isotope effect of benthic N₂ production. NO_x injected at greater depth is less likely to escape to the overlying water, since the oxic plume surrounding the burrow and the sediment-water interface are than separated by a larger reducing zone, where DNF and anammox take place. When the injected NO_x is quantitatively consumed DNF does not induce fractionation.

Our model results provide context for the interpretation of field observations. Lehmann *et al.* (2004) measured benthic N fluxes with incubation experiments in shelf sediments of the Santa Monica Bay, where bioirrigation plays an important role. They observed that the isotopic composition of NO_3^- did not change over time, which suggests that, similar to our baseline scenario, the NO_3^- was quantitatively consumed. In contrast, Dale *et al.* (2014) reported a strong benthic N isotope effect in hypoxic Mauritanian margin sediments. Their ε_{sed} value was -13% and appeared to be mostly communicated to the overlying water through NO_x exchange fluxes. On photographs of the sediments burrow openings and other signs of macrofaunal activity were visible, consistent with substantial

bioirrigation. Granger *et al.* (2011) estimated an ε_{sed} value of -6 to -8% based on measured light NO₃⁻ and heavy reduced N in bottom water of the Bering Sea shelf, and argued that partial nitrification of the benthic NH₄⁺ pool drove the N isotope effect of benthic N₂ production. The benthic infauna was not identified in their study, but burrows are prevalent in Bering Sea shelf sediments (Davenport *et al.*, 2012) exposed to large fluxes of POM (Baumann *et al.*, 2013). Large NH₄⁺ effluxes are common in bioirrigated sediments (Na *et al.*, 2008; Stief, 2013, Lehmann *et al.*, 2004) due to enhanced mineralization rates (Aller and Aller, 1998; Kristensen, 2001) and the ejection of anoxic porewater (Volkenborn *et al.*, 2010). Under these conditions, the N isotope effect of anammox and coupled nitrification-N₂ production can be communicated to the overlying water through effluxes of isotopically heavy NH₄⁺, which is consistent with our analysis (see for example the effect of higher mineralization rates in Figs. 3c and f).

The effect of bioirrigation can also be compared and contrasted with other transport regimes. Advective flow caused by pressure gradients, which may be the result of bottom currents over rippled sediment surfaces or the motion of waves, can lead to high N_2 production in sediments (Boudreau *et al.*, 2001b; Kessler *et al.*, 2012). Based on combined water-column experiments and modeling Kessler *et al.* (2014) estimated that benthic N_2 production in these sediments can lead to NO_3^- fluxing out of the sediment that is enriched by $3 \pm 1\%$. Nitrification did not occur in their experiment, but their model indicated that including nitrification would have a small effect. DNF under advective flow regimes is mainly driven by NO_3^- from the overlying water, while coupling between nitrification and DNF is low (Kessler *et al.*, 2012). This is in stark contrast to sediments with deeper bioirrigation, where the coupling between nitrification and N_2 production is strong as all the NO_x produced in the oxic plume surrounding the burrow is ultimately reduced to N_2 .

When the transport regime is dominated by diffusion, NO_x fluxing into the sediment will be quantitatively consumed. In such a setting, a benthic N isotopic effect can still occur if the isotopic composition of the NO_x fluxing into the sediment differs from that of bottom water NO_x . Models have indicated that the preferential consumption of light NO_x in the

sediment leads to a steeper gradient of ¹⁴NO_x than ¹⁵NO_x, which then results into a net flux of light NO_x into the sediment and consequently the in situ production of light N₂ (Bender, 1990; Brandes and Devol, 1997). However, early studies showed that the isotopic composition of NO_x in the overlying water did not change during incubation experiments, which could suggest that N isotope fractionation in the sediment was negligible (Brandes and Devol, 2002; Lehmann et al., 2007). It is also possible that the production of light NO_x during nitrification can mask the preferential use of isotopically light NO_x during DNF (Lehmann et al., 2007). This was observed in the simulation with bioirrigation turned off (Q = 0, Fig. 3a) where ε_{sed} was -12.6‰, while the sediment NO_x efflux was enriched by only 1.7%. The N isotope effect is then communicated to the overlying water primarily through the efflux of heavy NH₄⁺. Qualitatively, this is in agreement with a benthic N isotope effect of up to -7.2% modeled by Lehmann et al. (2007), who accounted for aerobic respiration, denitrification and nitrification only. It is also consistent with work by Dähnke and Thampdrup (2013), who showed experimentally that apparent N isotope fractionation during benthic DNF can occur in a setting where transport is dominated by diffusion. When diffusion is the only transport mechanism, a longer distance between the DNF zone and the sediment-water interface will decrease the benthic N isotope effect (Lehmann et al., 2007). Since this distance is dependent on the O_2 penetration depth, higher bottom water O_2 concentrations may cause less fractionation. However, higher O₂ bottom water concentrations can also be associated with a smaller benthic N isotope effect in bioirrigated sediments (Fig. 3d). This illustrates that the impact of O_2 on ε_{sed} not only depends on other biogeochemical factors such as mineralization rates but also on the transport mechanisms.

Benthic nitrogen isotope effects under commonly encountered environmental conditions

519 conditions520 Our simulations indicat

495

496

497

498

499

500

501

502

503

504

505

506

507

508

509

510

511

512

513

514

515

516

517

518

521

522

523

524

525

Our simulations indicate that the N isotope effect will be strongest in surficial sediments that have either strongly reducing or oxidizing conditions (Figs. 3a and 4). Redox conditions strongly depend on the intensity of bioirrigation and the reaction rates consuming O₂, reflected in mineralization rate. However, settings with high bioirrigation intensity and low mineralization rates or vice versa are relatively rare. These two competing factors commonly correlate, since OM rich settings with high rates of

mineralization can support a large number of benthic infauna (Künitzer *et al.*, 1992), which enhance the transport of oxidants into the sediment. Conversely, in areas where POM is scarce the bioirrigation intensity may be lower. By using the relationships between the bioirrigation intensity and benthic mineralization rates (see Eqns. 12 and 13) the model simulations predict that ε_{sed} values in bioirrigated sediment are commonly close to -3% (Fig. 4). However, there are a number of uncertainties associated with this estimate. Firstly, our simulations of shallower burrows indicate a larger benthic N isotope effect (Fig. 3b). However, smaller organisms are likely to pump less, and enhanced flow may also lead to conditions more comparable to the advective setting studied by Kessler *et al.* (2014). Secondly, N-cycling processes not considered in the model may also impact fractionation. Thirdly, comprehensive data sets on benthic N isotope cycling suitable for model parameterization are scarce, offering limited constraints on the model parameterization. For example, it is clear that fractionation factors in the field may differ from laboratory conditions, yet it is not well understood what causes the discrepancies between different studies (Kritee *et al.*, 2012).

Bioirrigation is important in shallow marine environments where a significant part of the global N_2 production takes places and therefore must have a large imprint on the global average N isotope effect of benthic N_2 production (ε_{glob}). Our estimate of -3% being common for bioirrigated sediments is akin to previous estimates of ε_{glob} . Lehmann *et al.* (2007) estimated -4%, which is remarkably similar given the fact that they did not account for advective transport and considered a different set of early diagenetic reactions. Kessler *et al.* (2014) also found an N isotope effect of $\sim -3\%$ for coastal sediment with transport dominated by wave-induced advection. Global circulation models coupled to N cycle models have tried to reproduce the measured NO_3^- concentrations and isotopic composition in the ocean to spatially resolve pelagic and benthic N_2 production rates. Using this approach, Somes *et al.* (2013) found best fits of the ocean fixed $\delta^{15}N$ with ε_{glob} values between -2 and -4%. Such benthic fractionation has a significant impact on estimates of benthic vs. pelagic N_2 production. Assuming steady-state and considering only nitrogen fixation as source and water-column and

benthic N_2 production as sinks, the fraction $f_{benthic}$ of benthic N_2 production of the total N_2 production can be estimated as

$$f_{benthic} pprox \frac{\varepsilon_{fix} - \delta^{15} N - N_{fix,avg} - \varepsilon_{wc}}{\varepsilon_{glob} - \varepsilon_{wc}}$$
 (15)

where ε_{fix} is the N isotope effect of N fixation ($\sim -1\%$), δ^{15} N-N_{fix,avg} is the average isotopic composition of ocean fixed N ($\sim 5\%$), and ε_{wc} is the N isotope effect of water-column N₂ production. Kritee *et al.* (2012), whose experiments indicated that turbulence and thermodynamically lower N isotope fractionation at the cell level, argued that ε_{wc} might fall in the range of -10 to -15%, which is substantially different from earlier estimates such as the -20% estimated by Brandes and Devol (2002). Furthermore, less apparent fractionation can be expected in oxygen minimum zones if NO₃⁻ becomes locally heavier than the average ocean δ_{NO3} (Deutsch *et al.*, 2004). Using ε_{wc} =-12.5% and ε_{glob} =-3%, leads to 68% of total marine N₂ production to taking place in the sediment. For water-column N₂ production of ~ 70 Tg N yr⁻¹ (Bianchi *et al.*, 2012), the benthic N₂ production rate would be 152 Tg N yr⁻¹. A $\pm 1\%$ uncertainty in ε_{glob} corresponds to global benthic N₂ production rates between 114 and 228 Tg N yr⁻¹, which highlight the sensitivity of the ocean fixed δ^{15} N towards N isotope fractionation in sediments.

Conclusion

Redox conditions exert a major control on the N isotope effect of benthic N₂ production, since they determine the extent to which different benthic N pools are consumed within the sediment. Fractionation against heavy NH₄⁺ during nitrification and anammox is enhanced under reducing conditions. Conversely, fractionation against heavy NO_x during DNF is enhanced under oxidizing conditions.

Solute transport processes together with the POM rain rate and the composition of the overlying water control the redox conditions in sediments. Bioirrigation can enhance mineralization (Aller and Aller, 1998; Kristensen, 2001), which promotes reducing conditions, but this effect is opposed by the injection of oxic water, which leads to more oxidizing conditions. The benthic N isotope effect is largest under either strongly

reducing or strongly oxidizing conditions, which correspond to combinations of low bioirrigation intensities and high mineralization rates and vice versa, or when shallow pumping leads to substantial recirculation of injected dissolved N. However, under conditions most commonly encountered in bioirrigated sediments, the benthic N isotope effect is estimated to be close to -3%, which is similar to previous estimates of the global N isotope effect (Lehmann *et al.*, 2007; Somes *et al.*, 2013). Such fractionation in sediments leads to substantially heavier NO_x in the ocean, tilting the balance towards benthic N₂ production, compared to estimates that ignore fractionation in marine sediments.

Acknowledgements: We would like to thank A.W. Dale and two anonymous reviewers for their constructive criticism and insightful comments, and T. Dornhoffer for his contributions to the bioirrigation model. This research was made possible in part by a grant from The Gulf of Mexico Research Initiative to support the "Ecosystem Impacts of Oil and Gas in the Gulf" (ECOGIG) research consortium, and in part by the U.S. National Science Foundation (OCE 0751882). Data are publicly available through the Gulf of Mexico Research Initiative Information & Data Cooperative (GRIIDC) at https://data.gulfresearchinitiative.org (doi: 10.7266/N7QR4V45). This is ECOGIG contribution no. 364.

607

- Alkhatib M., Lehmann M. F. and Del Giorgio P. A. (2012) The nitrogen isotope effect of
- benthic remineralization-nitrification-denitrification coupling in an estuarine
- environment. *Biogeosciences* **9**, 1633-1646.
- Aller R. C. and Aller J. Y. (1998) The effect of biogenic irrigation intensity and solute
- exchange on diagenetic reaction rates in marine sediments. J. Mar. Res. 56, 905-
- 613 936.
- Altabet M. A., Murray D. W. and Prell W. L. (1999) Climatically linked oscillations in
- Arabian Sea denitrification over the past 1 m.y.: Implications for the marine N
- 616 cycle. *Paleoceanography* **14**, 732-743.
- Archer D. and Devol A. H. (1992) Benthic oxygen fluxes on the Washington shelf and
- slope: A comparison of in situ microelectrode and chamber flux measurements.
- 619 *Limnol. Oceanogr.* **37**, 614-629.
- 620 Baumann M. S., Moran S. B., Kelly R. P., Lomas M. W. and Shull D. H. (2013) ²³⁴Th
- balance and implications for seasonal particle retention in the eastern Bering Sea.
- 622 Deep-Sea Res. 2 94, 7-21.
- Bender M. L. (1990) The $\delta^{18}O$ of dissolved O_2 in seawater: a unique tracer of circulation
- and respiration in the deep sea. J. Geophys. Res. 95, 22243–22252.
- Bianchi D., Dunne J. P., Sarmiento J. L. and Galbraith D. (2012) Data-based estimates of
- suboxia, denitrification, and N₂O production in the ocean and their sensitivities to
- dissolved O₂. Global Biogeochem. Cycles **26**, GB2009.
- Bohlen L., Dale A. W. and Wallman K. (2012) Simple transfer functions for calculating
- benthic fixed nitrogen losses and C:N:P regeneration ratios in global
- biogeochemical models. *Global Biogeochem. Cycles*, **26**, GB3029.
- Boudreau B. P. (1997) Diagenetic models and their implementation, 1st ed., Springer,
- Berlin.
- Boudreau B. P. (1996) The diffusive tortuosity of fine-grained unlithified sediments.
- 634 *Geochim. Cosmochim. Acta* **60**, 3139-3142.
- Boudreau, B. P. (2001a) Solute transport above the sediment-water interface. In:
- Boudreau B. P. and Jørgensen B. B. (eds), The Benthic Boundary Layer, Oxford
- University Press, New York, pp. 104–126.

- Boudreau B. P., Huettel M., Forster S., Jahnke R. A., McLaghlan A., Middelburg J. J.,
- Nielsen P., Sansone F., Taghon G., Van Raaphorst W., Webster I., Weslawski J.
- M., Wiberg P. and Sundby B. (2001b) Permeable Marine Sediments: Overturning
- and Old Paradigm. *EOS* **82**, 133-136.
- Brandes J. A., Devol A. H., Yoshinari T., Jayakumar D. A. and Nagyi S. W. A. (1998)
- Isotopic composition of nitrate in the central Arabian Sea and eastern tropical
- North Pacific: A tracer for mixing and nitrogen cycles. *Limnol. Oceanogr.* 43,
- 645 1680-1689.
- Brandes J. A. and Devol A. H. (1997) Isotopic fractionation of oxygen and nitrogen in
- coastal marine sediments. *Geochim. Cosmochim. Acta* **61**, 1793-1801.
- Brandes J. A. and Devol A. H. (2002) A global marine-fixed nitrogen isotopic budget:
- Implications for Holocene nitrogen cycling. *Global Biochem. Cycles* **16**, 1120.
- Brandes J. A. and Devol A. H. (1995) Simultaneous nitrate and oxygen respiration in
- coastal sediments: Evidence for discrete diagenesis. *J. Mar. Res.* **53**, 771-797.
- Brunner B., Contreras S., Lehmann M. F., Matantseva O., Rollog M., Kalvelage T.,
- Klockgether G., Lavik G., Jetten M. S. M., Kartal B. and Kuypers M. M. M.
- 654 (2013) Nitrogen isotope effects induced by anammox bacteria. PNAS.
- http://dx.doi.org/ 10/1073/pnas.1310488110.
- 656 Carpenter E., Harvey H., Fry B. and Capone D. (1997): Biogeochemical tracers of the
- marine cyanobacterium Trichodesmium. *Deep-Sea Res. 1* **44**, 27–38.
- 658 Casciotti K. L. (2009) Inverse kinetic isotope fractionation during bacterial nitrite
- oxidation. Geochim. Cosmochim. Acta 73, 2061-2076.
- Dähnke K. and Thamdrup B. (2013) Nitrogen isotope dynamics and fractionation during
- sedimentary denitrification in Boknis Eck, Baltic Sea. *Biogeosciences* **10**, 3079-
- 662 3088.
- Dale A. W., Sommer S., Ryabenko A., Noffke A., Bohlen L., Wallmann K., Stolpovsky
- K., Greinert J. and Pfannkuche O. (2014) Benthic nitrogen fluxes and
- fractionation of nitrate in the Mauritanian oxygen minimum zone (Eastern
- Tropical North Atlantic). *Geochim. Cosmochim. Acta* **134**, 234-256.
- D'Andrea A. F. and DeWitt T. H. (2009) Geochemical ecosystem engineering by the
- mud shrimp *Upogebia pugettensis* (Crustacea: Thalassinidae) in Yaquina Bay,

- Oregon: Density-dependent effects on organic matter remineralization and nutrient cycling. *Limnol. Oceanogr.* **54**, 1911-1932.
- Davenport E. S., Shull D. H. and Devol A. H. (2012) Roles of sorption and tube-dwelling
- benthos in the cycling of phosphorus in Bering Sea sediments. *Deep-Sea Res. 2*
- **65**, 163-172.
- Deutsch C., Sigman D. M., Thunell R. C., Meckler A. N. and Haug G. H. (2004) Isotopic
- constraints on glacial/interglacial changes in the oceanic nitrogen budget. *Global*
- 676 Biogeochem. Cycles 18, GB4012.
- Dornhoffer T. M., Waldblusser G. G. and Meile C. (2015) A modeling study of lugworm
- 678 irrigation behavior effects on sediment nitrogen cycling. Mar. Ecol. Prog. Ser.
- **534**, 121-134.
- Emery K. O. (1968) Relict sediments on continental shelves of the world. Am. Assoc. Pet.
- 681 *Geol. Bull.* **52**, 445-464.
- Fennel K., Brady D., DiToro D., Fulweiler R. W., Gardner W. S., Giblin A., McCarthy
- M. J., Rao A., Seitzinger S., Thouvenot-Korppoo M. and Tobias C. (2009)
- Modeling denitrification in aquatic sediments. *Biogeochemistry* **93**, 159-178.
- 685 Granger J., Sigman D. M., Lehmann M. F. and Tortell P. D. (2008) Nitrogen and oxygen
- isotope fractionation during dissimilatory nitrate reduction by denitrifying
- 687 bacteria. *Limnol. Oceanogr.* **53**, 2533–2545.
- 688 Granger J., Prokopenko M. G., Sigman D. M., Mordy C. W., Morse Z. M., Morales L.
- V., Sambrotto R. N. and Plessen B. (2011) Coupled nitrification-denitrification in
- sediment of the eastern Bering Sea shelf leads to ¹⁵N enrichment of fixed N in
- shelf waters. *J. Geophys. Res.* **116**, C11006.
- 692 Grundmanis V. and Murray J. W. (1977) Nitrification and denitrification in marine
- sediments from Puget Sound. *Limnol. Oceanogr.* **22**, 804-813.
- Hamersley M. R. and Howes B. L. (2004) Evaluation of the N₂ flux approach for
- measuring sediment denitrification. *Estuar. Coast. Shelf Sci.* **62**, 711-723.
- 696 Hüttel M. (1990) Influence of the lugworm Arenicola Marina on porewater nutrient
- profiles of sand flat sediments. *Mar. Ecol. Prog. Ser.* **62**, 241-248.
- 698 Hüttel M., Røy H., Precht E., and Ehrenhauss S. (2003) Hydrological impact on
- biogeochemical processes in aquatic sediments. *Hydrobiologia* **494**, 231-236.

- Jones S. E. and Jago C. F. (1993) In situ assessment of modification of sediment properties by burrowing invertebrates. *Mar. Biol.* **115**, 133-142.
- Kessler A. J., Glud R. N., Cardenas B., Larsen M., Bourke M. F. and Cook P. L. M.
- 703 (2012) Quantifying denitrification in rippled permeable sands through combined
- flume experiments and modeling. *Limnol. Oceanogr.* **57**, 1217-1232.
- Kessler A. J., Bristow L. A., Cardenas M. B., Glud R. N., Thamdrup B. and Cook P. L.
- 706 M. (2014) The isotope effect of denitrification in permeable sediments. *Geochim*.
- 707 *Cosmochim. Acta* **133**, 156-167.
- 708 Kristensen E. (2001) Impact of polychaetes (Nereis spp. and Arenicola marina) on
- carbon biogeochemistry in coastal marine sediments. *Geochem. Trans.* **2**, 92-103.
- 710 Kritee K., Sigman D. M., Granger J., Ward B. B., Jayakumar A. and Deutsch C. (2012)
- Reduced isotope fractionation by denitrification under conditions relevant to the
- 712 ocean. *Geochim. Cosmochim. Acta* **92**, 243-259.
- Künitzer A., Basford D., Craeymeersch J. A., Dewarumez J. M., Dörjes J., Duineveld G.
- 714 C. A., Eleftheriou A., Heip C., Herman P., Kingston P., Niermann U., Rachor E.,
- Rumohr H. and de Wilde P. A. J. (1992) The benthic infauna of the North Sea:
- species distribution and assemblages. *ICES J. Mar. Sci.* **49**, 127-143.
- 717 Le Bars M. and Worster G. (2006) Interfacial conditions between a pure fluid and a
- porous medium: implications for binary alloy solidification. J. Fluid Mech. 550,
- 719 149-173.
- 720 Lehmann M. F., Sigman D. M. and Berelson W. M. (2004) Coupling the ¹⁵N/¹⁴N of
- nitrate as a constraint on benthic nitrogen cycling. *Mar. Chem.* **88**, 1-20.
- Lehmann M. F., Sigman D. M., McCorkle D. C., Granger J., Hoffmann S., Cane G. and
- Brunelle B. G. (2007) The distribution of nitrate ¹⁵N/¹⁴N in marine sediments and
- the impact of benthic nitrogen loss on the isotopic composition of oceanic nitrate.
- 725 *Geochim. Cosmochim. Acta* **71**, 5384-5404.
- Lie U. (1968) A quantitative study of the benthic infauna in Puget Sound, Washington,
- 727 USA in 1963-64. FiskDir. Skr. Ser. HavUnders 14, 229-556.
- 728 Lønborg C. and Søndergaard M. (2009) Microbial availability and degradation of
- dissolved organic carbon and nitrogen in two coastal areas. Estuar. Coast. Shelf
- 730 *Sci.* **81**, 513-520.

- Mariotti A., Germon J. C., Hubert P., Kaiser P., Letolle R., Tardieux R. and Tardieux P.
- 732 (1981) Experimental determination of nitrogen kinetic isotope fractionation: some
- principles; illustration for the denitrification and nitrification processes. *Plant Soil*
- 734 **62**, 413–430.
- 735 Meile C. and Van Cappellen P. (2003) Global estimates of enhanced solute transport in
- marine sediments. *Limnol. Oceanogr.* **48**, 777-786.
- Meysman F. J. R., Middelburg J. J. and Heip C. H. R. (2006a) Bioturbation: a fresh look
- at Darwin's last idea. *Trends Ecol. Evol.* **21**, 688-695.
- 739 Meysman F. J. R., Galaktionov O. S., Gribsholt B. and Middelburg J.J. (2006b)
- Bioirrigation in permeable sediments: Advective pore-water transport induced by
- burrow ventilation. *Limnol. Oceanogr.* **51**, 142-156.
- Middelburg J. J., Soetaert K. and Herman P. M. J. (1997) Empirical relationships for use
- in global diagenetic models. *Deep-Sea Res. I* **44**, 327-344.
- Minagawa M. and Wada E. (1986) Nitrogen isotope ratios of red tide organisms in the
- East-China-Sea a characterization of biological nitrogen-fixation. *Mar. Chem.*
- 746 **19**, 245–259.
- Montoya J. P. (2008) Chapter 29: Nitrogen Stable Isotopes in Marine Environments. In:
- Capone D., Carpenter E., Mullholland M., and Bronk D. (eds), Nitrogen in the
- marine environment. Elsevier, Amsterdam, pp. 1277–1302.
- Na T., Gribsholt B., Galaktionov O. S., Lee T. and Meysman F. J. R. (2008) Influence of
- advective bio-irrigation on carbon and nitrogen cycling in sandy sediments. J.
- 752 *Mar. Res.* **66**, 691-722.
- 753 Nichols F. H. (2003) Interdecadal change in the deep Puget Sound benthos.
- 754 *Hydrobiologia* **493**, 95-114.
- 755 Pallud C. and Van Cappellen P. (2006) Kinetics of microbial sulfate reduction in
- estuarine sediments. *Geochim. Cosmochim. Acta* **70**, 1148-1162.
- Reitze M. and Schöttler U. (1989) The time dependence of adaption to reduced salinity in
- 758 the lugworm Arenicola marina L. (Annelida: Polychaeta). Comp. Biochem.
- 759 *Physiol.* **93**, 549-559.
- Riisgård H. U. and Banta G. T. (1998) Irrigation and deposit feeding by the lugworm
- 761 Arenicola marina, characteristics and secondary effects on the environment. A

- review of current knowledge. *Vie Milieu* **48**, 243-257.
- Sarmiento J. L. and Gruber N. (2006) Ocean Biogeochemical Dynamics. Princeton
- 764 University Press, Princeton.
- Shearer G., Schneider J. D. and Kohl D. H. (1991) Separating the efflux and influx
- components of net nitrate uptake by Synechococcus-R2 under steady-state
- 767 conditions. *J. Gen. Microbiol.* **137**, 1179–1184.
- Sigman D. M., Robinson R., Knapp A. N., van Geen A., McCorkle D. C., Brandes J. A.,
- and Thunell R. C. (2003) Distinguishing between water column and sedimentary
- denitrification in the Santa Barbara Basin using the stable isotopes of nitrate.
- 771 Geochem. Geophys. Geosyst. 4, 1040.
- Somes C. J., Oschlies A. and Schmittner A. (2013) Isotopic constraints on the pre-
- industrial oceanic nitrogen budget. *Biogeosciences* **10**, 5889-5910.
- 774 Stief P. (2013) Stimulation of microbial nitrogen cycling in aquatic ecosystems by
- benthic macrofauna: mechanisms and environmental implications. *Biogeosciences*
- **10**, 7829-7846.
- 777 Van Cappellen P. and Wang Y. F. (1995) Metal cycling in surface sediments: Modeling
- the interplay of transport and reaction. In: Allen H. E. (ed), Metal Speciation and
- 779 Contamination of Aquatic Sediments. Ann Arbor Press, Chelsea, Michigan, pp.
- 780 21-64.
- Volkenborn N., Hedtkamp S. I. C., Van Beusekom J. E. E. and Reise K. (2007) Effects of
- bioturbation and bioirrigation by lugworms (Arenicola Marina) on physical and
- chemical sediment properties and implications for intertidal habitat succession.
- 784 Estuar. Coast. Shelf Sci. **74**, 331-343.
- Volkenborn N., Polerecky L., Wethey D. S. and Woodin S. A. (2010) Oscillatory
- porewater bioadvection in marine sediments induced by hydraulic activities of
- 787 Arenicola marina. Limnol. Oceanogr. 55, 1231-1247.
- Wang Y. F. and Van Cappellen P. (1996) A multicomponent reactive transport model of
- early diagenesis: application to redox cycling in coastal marine sediment.
- 790 *Geochim. Cosmochim. Acta* **60**, 2993-3014.
- Wellman R. P., Cook F. D. and Krouse H. R. (1968) Nitrogen-15: Microbiological
- alteration of abundance. *Science* **161**, 269-270.

Tables and Figures

Table 1. Reactions and rate laws

Primary redox reactions*	
$({\rm CH_2O})_a({\rm NH_3})_b(aq) + a\;{\rm O_2} \rightarrow a\;{\rm CO_2} + f*b^{-14}{\rm NH_4}^+ + (1-f)*b^{-15}{\rm NH_4}^+ + a\;{\rm H_2O}$	$R_1 = k_{DOM} C_{DOM} \frac{c_{O_2}}{c_{O_2} + K_{m,O_2}}$
$(CH_2O)_a(NH_3)_b(aq) + 1.33a^{-14}NO_2^- + (1.33a + b) H^+ \rightarrow a CO_2 + f*b^{-14}NH_4^+ + (1-f)*b^{-15}NH_4^+ + 0.66a^{-14}N_2 + 1.66a H_2O$	$R_2^l = (k_{DOM}C_{DOM} - R_1) \frac{c_{14_{NO_2}}}{c_{14_{NO_2}} + c_{15_{NO_2}} + K_{m,NOx}}$
$(CH_2O)_a(NH_3)_b(aq) + 1.33a^{-15}NO_2^- + (1.33a + b) H^+ \rightarrow a CO_2 + f*b^{-14}NH_4^+ + (1-f)*b^{-15}NH_4^+ + 0.66a^{-15}N_2 + 1.66a H_2O$	$R_2^h = \alpha_{NO2,DNF}(k_{DOM}C_{DOM} - R_1) \frac{c_{15}_{NO_2^-}}{c_{14}_{NO_2^-} + c_{15}_{NO_2^-} + K_{m,NOX}}$
$(CH_2O)_a(NH_3)_b(aq) + 2a^{14}NO_3^- + b H^+ \rightarrow a CO_2 + f*b^{14}NH_4^+ + (1-f)*b^{15}NH_4^+ + 2a^{14}NO_2^- + a H_2O$	$R_3^l = (k_{DOM}C_{DOM} - R_1 - R_2^l - R_2^h) \frac{c_{14_{NO_3}^-}}{c_{14_{NO_3}^-} + c_{15_{NO_3}^-} + \kappa_{m,NOx}}$
$(CH_2O)_a(NH_3)_b(aq) + 2a^{15}NO_3^- + b H^+ \rightarrow a CO_2 + f*b^{14}NH_4^+ + (1-f)*b^{15}NH_4^+ + 2a^{15}NO_2^- + a H_2O$	$R_3^h = (k_{DOM}C_{DOM} - R_1 - R_2^l - R_2^h) \frac{c_{15_{NO_3}^-}}{c_{14_{NO_3}^-} + c_{15_{NO_3}} + \kappa_{m,NOx}}$
$(CH_2O)_a(NH_3)_b(aq) + 4a Fe(OH)_3 + (8a + b) H^+ \rightarrow a CO_2 + f*b^{14}NH_4^+ + (1-f)*b^{15}NH_4^+ + 4a Fe^{2+} + 11a H_2O$	$R_4 = (k_{DOM}C_{DOM} - R_1 - R_2^l - R_2^h - R_3^l - R_3^h) \frac{c_{Fe(OH)_3}}{c_{Fe(OH)_3} + k_{m,Fe(OH)_3}}$
$(CH_2O)_a(NH_3)_b(aq) + 0.5a SO_4^{2-} + (0.5a + b) H^+ \rightarrow a CO_2 + f*b^{14}NH_4^+ + (1-f)*b^{15}NH_4^+ + 0.5a HS^- + a H_2O$	$R_5 = (k_{DOM}C_{DOM} - R_1 - R_2^l - R_2^h - R_3^l - R_3^h - R_4) \frac{c_{SO_4^{2-}}}{c_{SO_4^{2-} + K_{m,SO_4}}}$
Other reactions	
$^{14}\text{NH}_4^+ + ^{14}\text{NO}_2^- \rightarrow ^{14}\text{N}_2 + 2 \text{ H}_2\text{O}$	$R_6^{ll} = k_{amx} C_{14NO_2^-} \frac{C_{14NH_4^+}}{C_{14NH_4^+} + C_{15NH_4^+} + K_{m,NH_4}}$
$^{14}\text{NH}_4^+ + ^{15}\text{NO}_2^- \rightarrow ^{14}\text{N}^{15}\text{N} + 2\text{ H}_2\text{O}$	$R_6^{NO2h} = \alpha_{NO2,amx} k_{amx} C_{15}{}_{NO_2^-} \frac{C_{14}{}_{NH_4^+}}{C_{14}{}_{NH_4^+} + C_{15}{}_{NH_4^+} + K_{m,NH_4}}$

$$R_{6}^{NH4^{+} + 14}NO_{2}^{-} \rightarrow {}^{14}N^{15}N + 2 \text{ H}_{2}O$$

$$R_{6}^{NH4h} = \alpha_{NH4,amx}k_{amx}C_{14}NO_{2}^{-} \frac{c_{15}NH_{4}^{+} + C_{15}NH_{4}^{+} + K_{m,NH4}}{c_{14}NH_{4}^{+} + C_{15}NH_{4}^{+} + C_{15}NH_{4}^{+} + K_{m,NH4}}$$

$$R_{6}^{hh} = \alpha_{NO2,amx}\alpha_{NH4,amx}k_{amx}C_{15}NO_{2}^{-} \frac{c_{15}NH_{4}^{+} + C_{15}NH_{4}^{+} + K_{m,NH4}}{c_{14}NH_{4}^{+} + C_{15}O_{2} + 2 \text{ HCO}_{3}^{-}} \rightarrow {}^{14}NO_{2}^{-} + 3 \text{ H}_{2}O + 2 \text{ CO}_{2}$$

$$R_{7}^{h} = \alpha_{NH4,ox}k_{AO}C_{O_{2}} \frac{c_{14}NH_{4}^{+} + C_{15}NH_{4}^{+} + K_{m,NH4}}{c_{15}NH_{4}^{+} + C_{15}NH_{4}^{+} + K_{m,NH4}}$$

$$R_{7}^{h} = \alpha_{NH4,ox}k_{AO}C_{O_{2}} \frac{c_{14}NH_{4}^{+} + C_{15}NH_{4}^{+} + K_{m,NH4}}{c_{15}NH_{4}^{+} + K_{m,NH4}}$$

$$R_{8}^{h} = k_{NO}C_{O_{2}}C_{14}NO_{2}^{-}$$

$$R_{8}^{h} = k_{NO}C_{O_{2}}C_{14}NO_{2}^{-}$$

$$R_{8}^{h} = \alpha_{NO2,ox}k_{NO}C_{O_{2}}C_{15}NO_{2}^{-}$$

$$R_{8}^{h} = \alpha_{NO2,ox}k_{NO}C_{O_{2}}C_{15}NO_{2}^{-}$$

$$R_{9} = k_{HS}C_{O_{2}}C_{HS}^{-}$$

$$R_{11} = \max\left(0, k_{FeS} \left[\frac{c_{Fe}^{2+}C_{HS}^{-}}{K_{FeS}C_{H}^{+}} - 1\right]\right)$$

$$(CH_{2}O)_{0}(NH_{3})_{b}(s) \rightarrow (CH_{2}O)_{3}(NH_{3})_{b}(aq)$$

$$R_{12} = F_{DOM,prod}/L$$

*(CH₂O)_a(NH₃)_b(aq) and (CH₂O)_a(NH₃)_b(s) refer to dissolved and particulate organic matter, respectively. 'a' and 'b' subscripts refer to the C:N ratio in organic matter, which was set to 106:16. 'f' denotes the fraction of ¹⁴N in organic matter ($f=^{14}N:[^{15}N+^{14}N]$). L refers to the length of the modeled sediment domain, which is 20 cm.

 Table 2. Parameters used in reaction-transport model (baseline)

Description	Symbol	Value or	Source
		Expression	
Environmental parameters			
Bottom water O ₂ concentration	$O_{2,bw}$	150 μΜ	a
Bottom water NO ₃ ⁻ concentration	$NO_3^{}_{,bw}$	23 μΜ	a
Isotopic composition bottom water NO ₃	$\delta^{15} N\text{-NO}_{3,bw}$	7.6‰	a
Isotopic composition organic N	Org. $\delta^{15}N$	7.0‰	a
Bottom water DOM concentration	$\mathrm{DOM}_{\mathrm{bw}}$	50 μΜ	b
Injected O ₂ concentration	$\mathrm{O}_{2,\mathrm{inj}}$	$0.4 * O_{2,bw}$	c
Injected NH ₄ ⁺ concentration	$\mathrm{NH}_{4,inj}$	8 μΜ	d
Imposed Fe(OH) ₃ concentration	Fe(OH) ₃	5 mM	
N:C of POM and DOM	N:C	16:106	
Porosity	Φ	0.4	
Acidity	pН	8.1	
In situ DOM production	$F_{\text{DOM,prod}}$	$4 \; mmol \; C \; m^{-2} \; d^{-1}$	e
Pumping rate	Q	0.62 mL min ⁻¹	e
Rate constants			
DOM production	k_{DOM}	$2 * 10^{-5} s^{-1}$	f
Anammox	k_{amx}	$1.7 * 10^{-5} \mathrm{s}^{-1}$	e
NH ₄ ⁺ oxidation	k_{AO}	$1.5 * 10^{-5} \mathrm{s}^{-1}$	e
NO ₂ ⁻ oxidation	k_{NO}	$6.3 * 10^{-7} \mu M^{-1} s^{-1}$	e
HS ⁻ oxidation	k_{HS}	$5.1 * 10^{-9} \mu M^{-1} s^{-1}$	g
Fe ²⁺ oxidation	k_{Fe}	$7.5 * 10^{-5} \mu M^{-1} s^{-1}$	h
FeS precipitation	k_{FeS}	$1.9 * 10^{-12} \mu M^{-1} s^{-1}$	g
Half-sat. constant aerobic respiration	$K_{m,O2}$	8 μΜ	g
Half-sat. constant DNF	$K_{m,NOx}$	12 μΜ	g
Half-sat. constant Fe(OH) ₃ reduction	$K_{\text{m,Fe}(\mathrm{OH})3}$	$50 * 10^3 \mu M$	h
Half-sat. constant SO_4^{2-} reduction	$K_{m,SO4}$	850 μΜ	i
Half-sat. constant anammox and $\mathrm{NH_4}^+$ oxidation	$K_{m,NH4}$	10 μΜ	e
Dissociation constant FeS	K_{FeS}	1.12 mM	g
Fractionation factors:			
Denitrification (NO ₂ ⁻)	$lpha_{ ext{NO2,DNF}}$	0.985	j
Denitrification (NO ₃ ⁻)	$\alpha_{ m NO3,DNF}$	0.979	j
Nitrification (NH ₄ ⁺)	$lpha_{ m NH4,ox}$	0.984	e

Nitrification (NO ₂ ⁻)	$\alpha_{NO2,ox}$	1.013	j
Anammox (NO_2^-)	$\alpha_{NO2,amx}$	0.982	k
Anammox (NH ₄ ⁺)	$lpha_{NH4,amx}$	0.984	e

Sources: a) Brandes and Devol (1997), b) Lønborg and Søndergaard (2009), c) Volkenborn *et al.* (2010), d) Reitze and Schöttler (1989), e) fitted to reproduce measurements of Brandes and Devol (1997), f) Dornhoffer *et al.* (2015), g) Wang and Van Cappellen (1996), h) Van Cappellen and Wang (1995), i) Pallud and Van Cappellen (2005), j) from data compiled by Casciotti (2009), k) Brunner *et al.* (2013).

Figure captions

- Fig 1. Steady-state concentration fields and reaction rates from the baseline simulation. The contours in panel b show the NO_x concentrations of the simulation with a feeding pocket at 5 cm depth. The concentrations and rates in panels c and f, respectively, are horizontally averaged over the domain.
- Fig. 2. Nitrogen cycling in the baseline simulation, a) N fluxes and their isotopic composition: measurements of Brandes and Devol (1997) are underlined; 'resp. worm' refers to NH₄⁺ produced during respiration by the worm, b) NO_x concentration and associated isotope signature in a benthic chamber reflecting the conditions of Brandes and Devol (1997). Lines are calculated from fluxes of the baseline (solid) and sensitivity analysis of DOM reactivity (dashed), while filled circles represent the observations of Brandes and Devol (1997).
- Fig. 3. Sensitivity of the N_2 production rate (mmol m⁻² d⁻¹) and benthic N isotope effect towards a) the pumping rate, b) the domain radius with a burrow depth of 15 cm and 5 cm, c) the reactivity of dissolved organic matter, d) the bottom water O_2 concentration, e) the bottom water NO_3^- concentration, and f) the in situ dissolved organic matter production rate. Stacked bars show the contribution of individual processes (see also Eq. 11). Asterisks indicate the values used in the baseline simulation.
- Fig. 4. The combined effect of the mineralization rate and bioirrigation intensity on the benthic N isotope effect (ε_{sed} , solid contour lines). The dashed line corresponds to Eq. 12. The dotted contour delineates the region in which the model computed N₂ flux is within \pm 10% of Eq. 13.

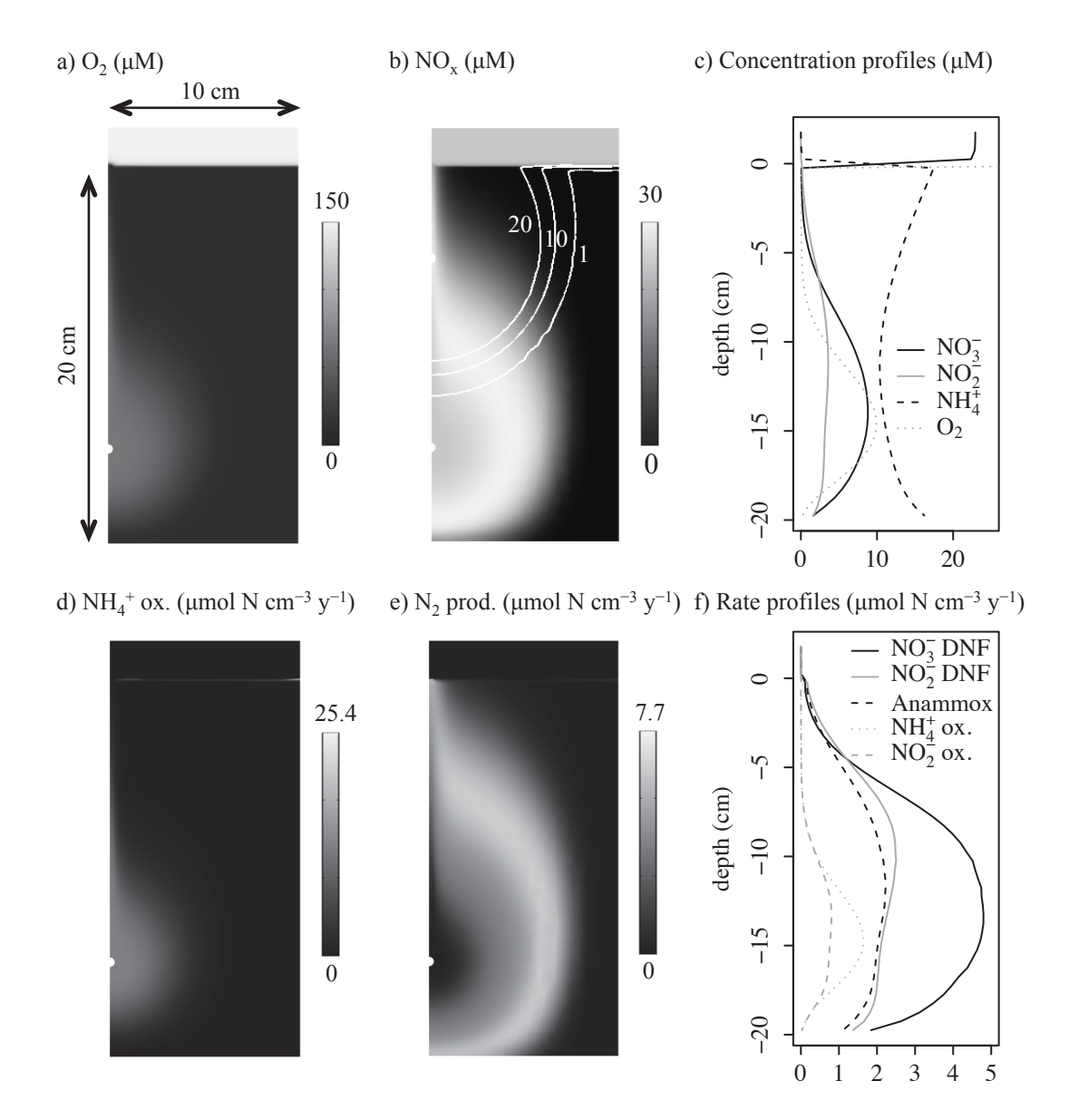


figure 1

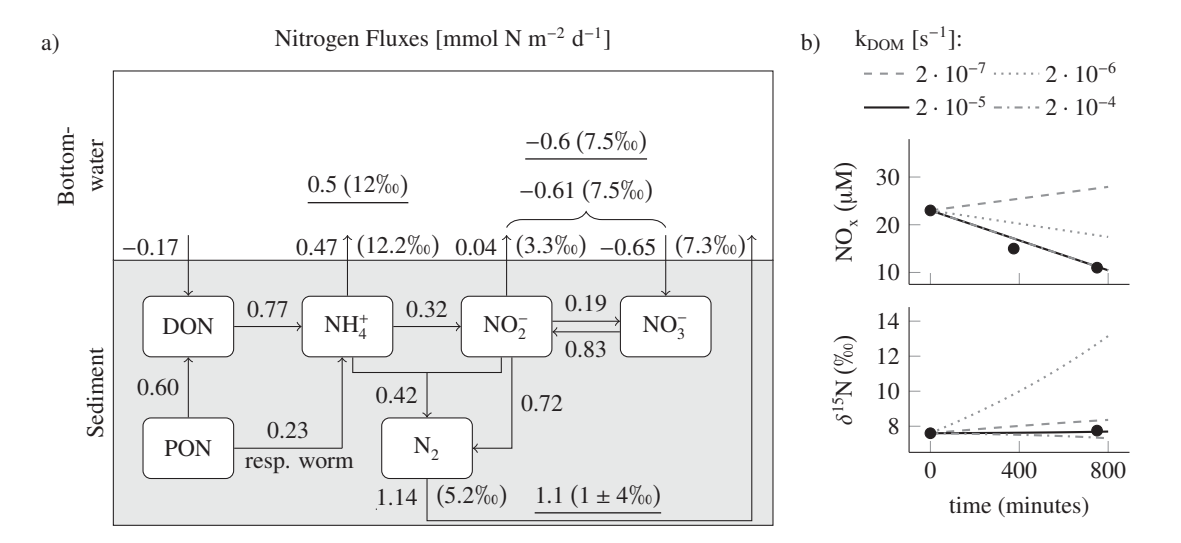


figure 2

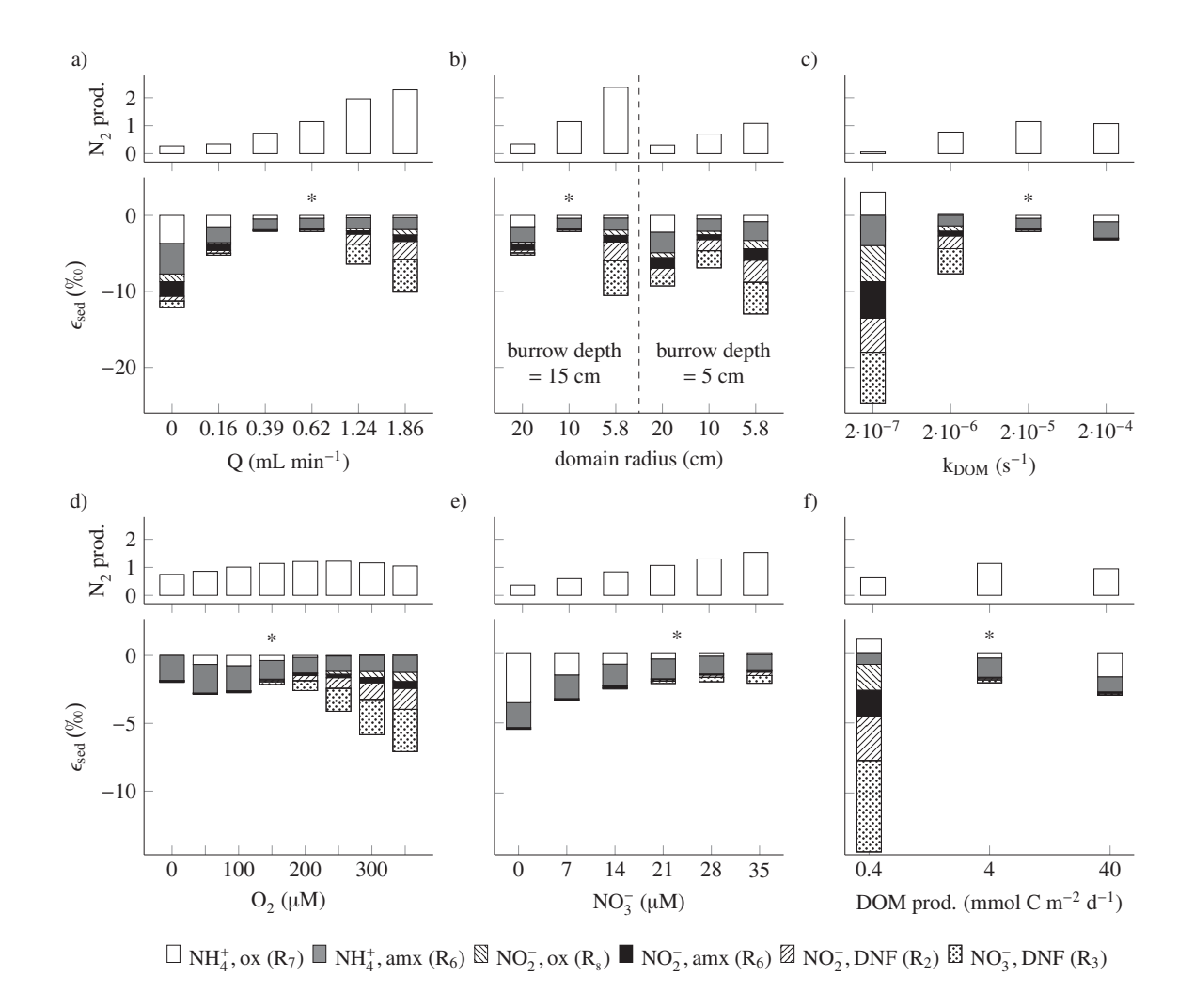


figure 3

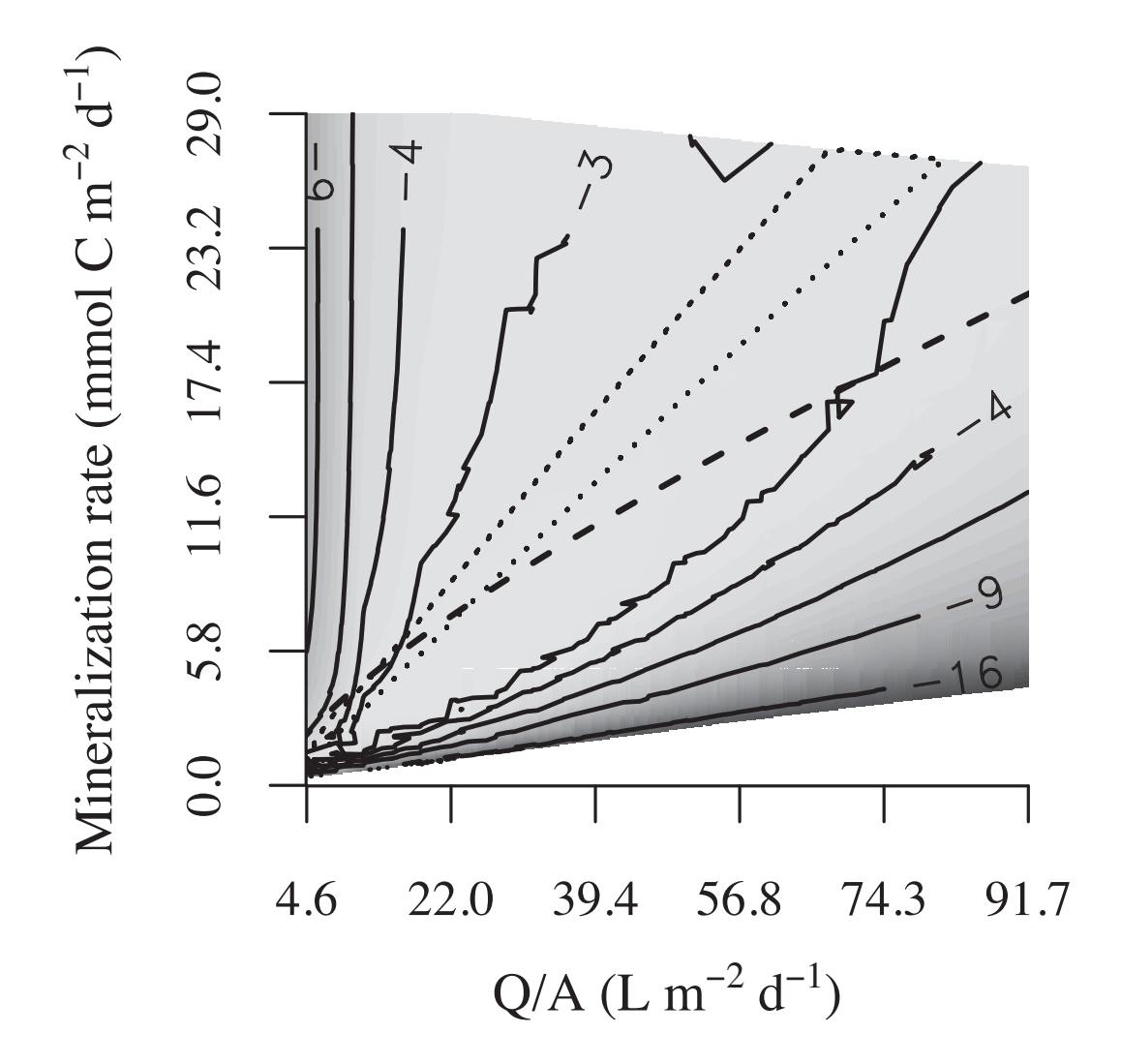


figure 4